Structures of Large Protein Complexes Determined by Nuclear Magnetic Resonance Spectroscopy

Chengdong Huang and Charalampos G. Kalodimos

Department of Biochemistry, Molecular Biology, and Biophysics, University of Minnesota, Minneapolis, Minnesota 55455; email: ckalodim@umn.edu

Annu. Rev. Biophys. 2017. 46:317–36

First published online as a Review in Advance on March 17, 2017

The *Annual Review of Biophysics* is online at biophys.annualreviews.org

https://doi.org/10.1146/annurev-biophys-070816-033701

Keywords

biomolecular NMR, protein–protein complexes, protein dynamics, large protein complexes

Abstract

Nuclear magnetic resonance (NMR) spectroscopy has been instrumental during the past two decades in providing high-resolution structures of protein complexes. It has been the method of choice for determining the structure of dynamic protein complexes, which are typically recalcitrant to other structural techniques. Until recently, NMR spectroscopy has yielded structures of small or medium-sized protein complexes, up to approximately 30–40 kDa. Major breakthroughs during the past decade, especially in isotope-labeling techniques, have enabled NMR characterization of large protein systems with molecular weights of hundreds of kDa. This has provided unique insights into the binding, dynamic, and allosteric properties of large systems. Notably, there is now a slowly but steadily growing list of large, dynamic protein complexes whose atomic structure has been determined by NMR. Many of these complexes are characterized by a high degree of flexibility and, thus, their structures could not have been obtained using other structural methods. Especially in the field of molecular chaperones, NMR has recently provided the first-ever high-resolution structures of their complexes with unfolded proteins. Further technological advances will establish NMR as the primary tool for obtaining atomic structures of challenging systems with even higher complexity.

Contents

INTRODUCTION

Almost all biological processes rely on proteins interacting and assembling into complexes (40). Given that the majority of proteins in the cell function by forming large assemblies, information on such complexes is vital to understanding the mechanisms underlying their function (1, 47, 81). Exciting advances in X-ray crystallography and, most recently, electron microscopy have played a major part in obtaining high-resolution structures of large protein complexes (59). However, a large number of protein assemblies that are dynamic have been recalcitrant to structural determination. These are complexes with fast association or dissociation kinetics, in which one or more of the partners is flexible—for example, unfolded or intrinsically disordered proteins—or retains a significant degree of flexibility in the complex or undergoes rapid conformational rearrangement in the complex (6, 9, 26, 41, 44, 69, 72). Nuclear magnetic resonance (NMR) spectroscopy is ideally suited to studying such dynamic complexes but has, until recently, been limited to complexes of low molecular weight (up to approximately 35 kDa).

The application of NMR spectroscopy to supramolecular systems has been revolutionized by advances in NMR instrumentation, pulse sequences, and, especially, isotope-labeling techniques, such as the specific labeling of methyl-bearing and aromatic residues (24, 31, 32, 46, 56). The methyl groups have some very favorable properties that render them excellent reporters of structure and dynamics in proteins: (*a*) They occur frequently in the hydrophobic cores of proteins or at the interfaces of biomolecular complexes; (*b*) they are very sensitive because the three protons of the methyl group all contribute to the intensity of the same signal; and (*c*) methyl groups are intrinsically optimized for use in TROSY (transverse relaxation optimized spectroscopy), and the simple ^{1}H-^{13}C HMQC (heteronuclear multiple quantum coherence) experiment can be used to select for pathways with favorable relaxation properties (31). Currently, the methyl groups of six amino acids can be labeled in a highly specific manner without scrambling: Ala, Ile, Leu, Met, Thr, and Val (32, 45, 71). In addition, the availability of aromatic residues specifically labeled in their rings (24, 29, 43, 68) provides a means for using them in larger protein systems. This is particularly important for characterizing protein complexes because protein interfaces are enriched in aromatic residues (79). The six methyl-bearing and aromatic residues are highly abundant, typically accounting for 45–55% of the total number of residues in a protein; they are distributed throughout the protein and, thus, provide almost complete coverage of the protein space.

The methyl and aromatic labeling scheme has been extensively employed during the past two decades to tackle large protein systems using NMR. The structures of several large proteins (up to approximately 80 kDa) have been determined, including membrane proteins (19, 54, 70, 75). Despite the challenge, resonance assignments for several supramolecular protein systems (with

molecular weights larger than 200 kDa) have been reported (14, 32, 64, 75). The availability of the assignments has enabled detailed NMR studies of these systems, and these have provided unique insights into their binding, dynamics, and allosteric properties (22, 36, 39, 56, 58, 73, 74, 84). More recently, the structures of a number of large, dynamic protein complexes have been determined by NMR. We review these systems, showcasing why NMR is ideally suited to determining the structure of large complexes that have a high degree of flexibility. The Hsp90–Tau system (27) provides an example of a structural model of a dynamic complex that was determined using docking and driven primarily by NMR chemical shift perturbation (CSP) data. The SecA signal sequence (14), and the nucleosome–HMGN2 (high mobility group nucleosomal 2) (30), ClpB–DnaK (57), and box C/D ribonucleoprotein enzyme (35) systems provide examples of complexes whose structures were determined by leveraging crystal structures of the unliganded proteins. Finally, the trigger factor (TF) (62) and SecB (21) chaperones bound to non-native proteins provide examples of large protein complexes whose structure was obtained using a large number of NOE (nuclear Overhauser effect) data to determine high-resolution structures de novo.

THE HSP90–TAU COMPLEX

Hsp90 is a molecular chaperone expressed at high levels in cells and is involved in the folding, stabilization, activation, and assembly of a large set of client proteins (37, 52). Hsp90 forms a dimer, with each protomer consisting of three domains: the N-terminal domain ATPase (N domain), the middle domain (M domain), and the C-terminal domain (C domain), which mediates dimerization (3, 11, 53). Structural studies revealed that ATP binding and hydrolysis in the N domain trigger a dramatic conformational change that spreads throughout the whole Hsp90 molecule, especially in the N and M domains (34, 65). Hsp90 is a major target for cancer therapeutics, resulting from the fact that many of its client proteins are involved in oncogenic processes (66). However, it remains poorly understood how the Hsp90 chaperone accommodates such a large diversity of client proteins (78).

To gain insight into the binding mechanisms of Hsp90 for its client proteins, Stefan Rüdiger's lab (27, 28) applied methyl TROSY methods to characterize the interaction of Hsp90 with Tau. Tau is an intrinsically disordered protein that has been associated with neural toxicity in Alzheimer's disease (23). The Tau binding site on Hsp90 was identified by monitoring the chemical shift in methyl TROSY spectra of Ile-labeled Hsp90 (**Figure 1*a***) upon the addition of unlabeled Tau (**Figure 1*b*,*c***). NMR spectral analysis revealed an approximately 100-Å-long substrate binding surface on Hsp90, spanning both the N and M domains. Such a large binding surface might allow for multiple low-affinity interactions between Hsp90 and Tau. Interestingly, the NMR signals were observed to split upon Tau binding, both in the nucleotide-free and the ATP-bound states of Hsp90, indicating that Tau binding breaks the symmetry of the Hsp90 dimer (**Figure 1*d***). CSP analysis demonstrated that Hsp90 binds to a 170-residue segment in Tau, with moderate hydrophobicity and a net positively charged nature. The CSP data about the interaction, combined with data from small-angle X-ray scattering (SAXS) and the crystal structural of apo Hsp90 (nucleotide-free Hsp90), allowed the authors (27) to build a structural model for the Hsp90–Tau complex using a docking approach. In this model, the Hsp90–Tau complex adopts an extended and dynamic conformation, with the binding region of Tau converged on the large, extended client binding surface of Hsp90 while the unbound Tau segments are dynamic (**Figure 1*e***). The authors argued that their results provide an explanation for how Hsp90 specifically selects for late-folding intermediates and also for some intrinsically disordered proteins, as both contain exposed stretches with scattered hydrophobic residues.

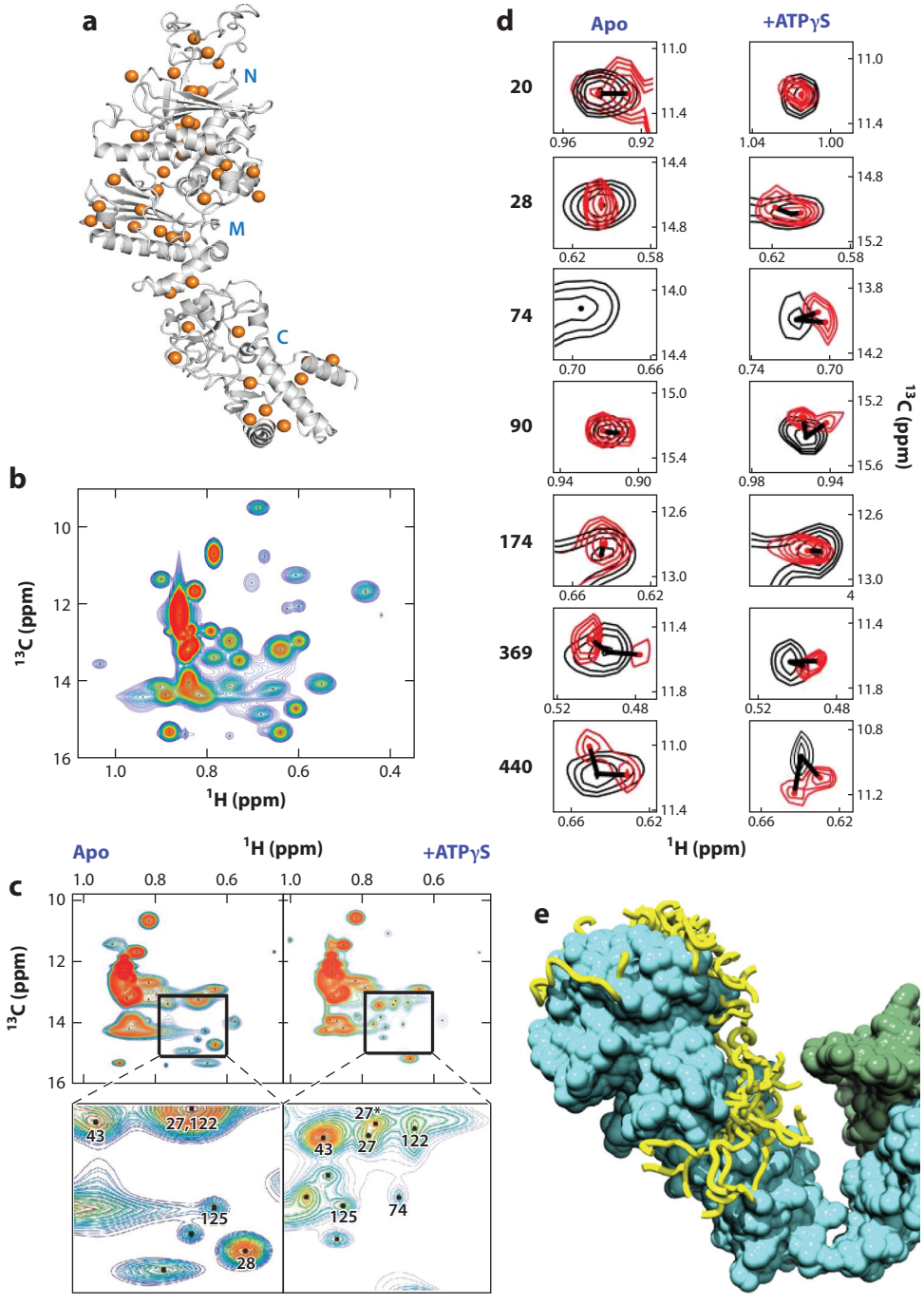
a
N
M
C
b
^{13}C (ppm)
^{1}H (ppm)
c
Apo
+ATPγS
^{1}H (ppm)
^{13}C (ppm)
43
27,122
125
28
27*
27
122
74
d
Apo
+ATPγS
20
28
74
90
174
369
440
^{13}C (ppm)
^{1}H (ppm)
e

THE SecA–SIGNAL SEQUENCE COMPLEX

Measuring intermolecular nuclear Overhauser enhancements (NOEs) in large protein complexes is challenging. A more straightforward approach to obtaining intermolecular distance restraints, albeit only long-range restraints (approximately 14–28 Å) (which result in less-well-defined structures than when NOE-derived distances are used), is to use the paramagnetic relaxation enhancement (PRE) technique (10). By combining transferred NOESY, line-broadening, and PRE experiments, our group determined the structure of the 204-kDa SecA ATPase in complex with a secretory signal peptide (**Figure 2**) (49). The structure of the complex was determined using NMR-driven simulated annealing of the signal peptide in the presence of the X-ray structure of free *Escherichia coli* SecA (49). Distance restraints between SecA and the signal peptide were obtained by combining site-directed spin labeling with NMR-detected PRE rates (**Figure 2**). Intermolecular distances up to approximately 28 Å could be measured. Because of the large density of methyl probes close to the peptide binding site, a large number of SecA–signal peptide distance restraints were obtained. Spin labels were engineered at different positions in the signal peptide by converting a single amino acid to Cys, to which a nitroxide spin label was attached. Two positions that were observed to give the most reliable data were K7C at the N terminus and Q25C at the C terminus. Placing the spin label in these positions, rather than closer to the termini, significantly decreased the mobility of the spin label, thus reducing nonspecific broadening. Placing the spin label in two different positions in the N and C termini of the peptide not only increased the number of distance restraints by roughly twofold but also contributed to better determination of the relative orientation of the peptide bound to SecA. The structure of the signal peptide in complex with SecA was determined by transferred NOESY and differential line-broadening experiments. The conformation of the peptide bound to SecA was probed by measuring NOEs within the peptide in the presence of a small amount of SecA. The data showed that although the free peptide is unstructured, its hydrophobic region (residues Leu13–Val21) adopts an α-helical conformation when interacting with SecA. The structure of the peptide bound to SecA was determined using 50 intramolecular NOEs. The best 10 structures of the peptide were then docked to SecA to determine the structure of the complex using the crystal structure of apo SecA as the starting conformation.

Figure 1

Nuclear magnetic resonance (NMR) studies of Hsp90 interaction with Tau and model structures of the Hsp90–Tau complex. (*a*) Distribution of Ile-δ1 methyl groups (*orange spheres*) in the human Hsp90β structure. The model of human Hsp90β was generated using the SWISS-MODEL website (Biozentrum, University of Basel; **https://swissmodel.expasy.org/**) and the crystal structure of *Escherichia coli* Hsp90 (Protein Data Bank identification number 2IOQ) as the template. Only one Hsp90 protomer is shown. N, M, and C indicate domains. (*b*) Methyl TROSY spectrum of the Ile-δ1 methyls of apo Hsp90. (*c*) ATP binding modulates the dynamics of the Hsp90–Tau complex. Shown is a rainbow representation of methyl TROSY (transverse relaxation optimized spectroscopy) spectra of Ile-methyl–bearing full-length Hsp90 in complex with unlabeled Tau in the absence of ATPγS (*left*) or its presence (*right*). Assigned residues are labeled. The binding of Tau causes a decrease in the NMR spectral intensity of Hsp90 (*left*), and ATPγS binding (*right*) dramatically sharpens the NMR signals of the Hsp90–Tau complex, indicating that the dynamics of the Hsp90–Tau complex are modulated by ATPγS binding. (*d*) The binding of Tau causes shifts and splits in some NMR signals of Hsp90 (Hsp90, 125 μM; Tau, 287 μM) (Hsp90, *black*; Hsp90 + Tau, *red*) in the absence of 2 mM ATPγS (*left*) and in its presence (*right*). The extent of each shift is indicated by a line. Analysis of the affected residues reveals that Tau binds to the N and M domains of Hsp90. Notably, the splitting of NMR signals upon Tau binding was observed in both the nucleotide-free (apo) and the ATP-bound states of Hsp90, indicating that Tau binding breaks the symmetry of the Hsp90 dimer. (*e*) Model of the Hsp90–Tau complex derived from NMR titration and small-angle X-ray scattering. The 10 best models indicate the convergence of Tau (*yellow*) on Hsp90 (two Hsp90 protomers are labeled in *cyan* and *green*). This model indicates that Tau-bound Hsp90 adopts an open V-shaped conformation; the Tau-binding site covers a remarkably extended surface, running along the N and M domains. Panel *b* reproduced with permission from Reference 29, copyright 2011, National Academy of Sciences, USA.

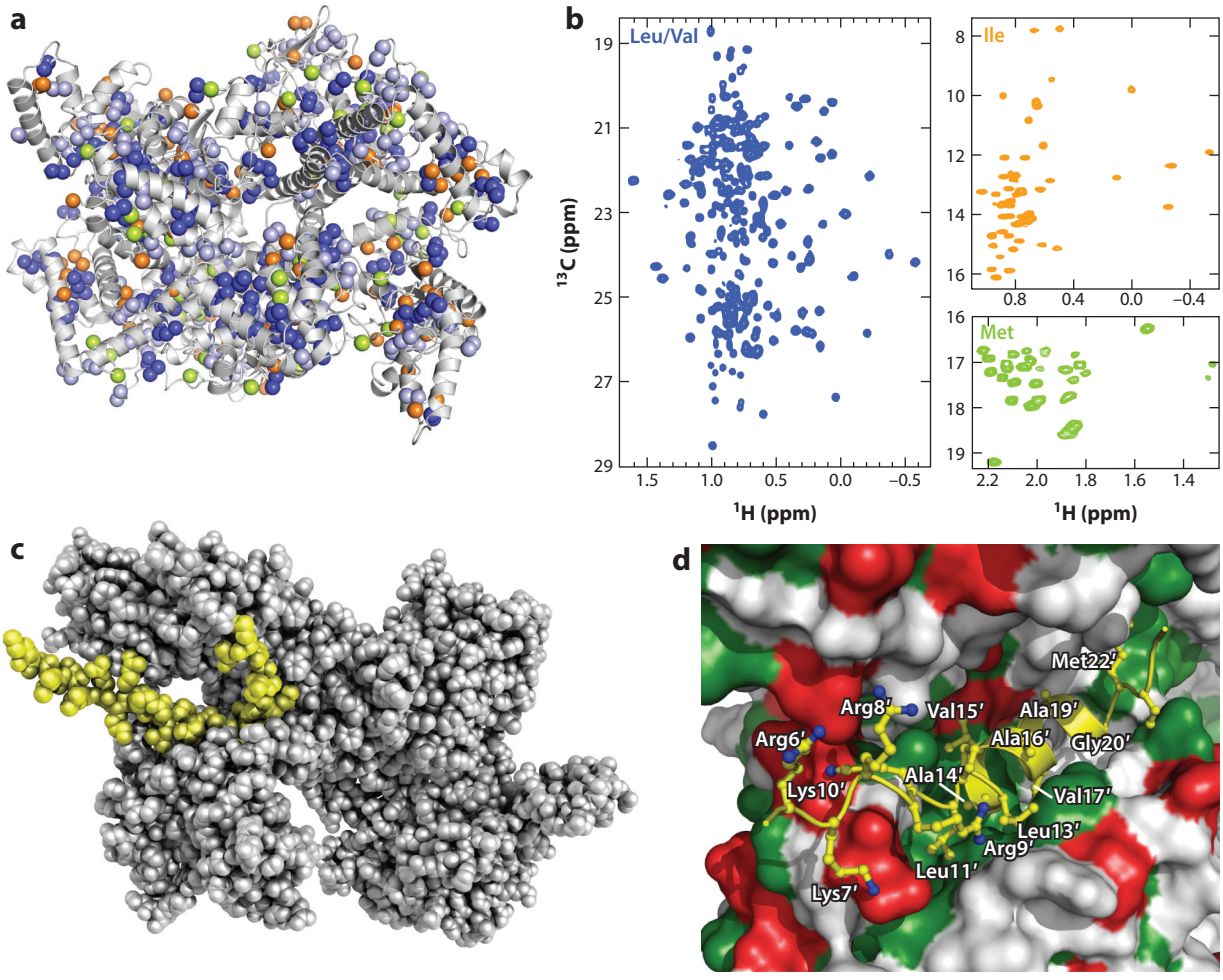

Figure 2

Nuclear magnetic resonance (NMR) characterization of the complex between SecA and the LamB signal peptide. (*a*) Distribution of methyl groups, displayed as spheres, in the dimeric *Escherichia coli* SecA. Residues are represented by the following colors (with the number of residues per subunit): Ile, orange (54 residues); Leu, dark blue (82 residues); Val, light blue (59 residues); and Met, green (33 residues). (*b*) ^{1}H-^{13}C HMQC (heteronuclear multiple quantum coherence) spectra of SecA U-[^{2}H,^{12}C],Val, Leu-[$^{13}CH_3$,$^{12}CD_3$], Ile-δ1-[$^{13}CH_3$], and Met-[$^{13}CH_3$]. All resonances expected on the basis of the number of labeled methyl-bearing residues are present. (*c*) The lowest-energy structure of SecA bound to the LamB signal peptide is shown. Both SecA (*white*) and the peptide (*yellow*) are displayed as spheres. The structural data demonstrate that the signal peptide binds into a relatively large groove formed at the interface of two domains. The structure was determined using the crystal structure of apo SecA (nucleotide-free SecA), and the peptide was docked by means of approximately 160 intermolecular distance restraints measured by NMR paramagnetic relaxation enhancement experiments. The structure of the bound peptide was determined using transferred NOESY (nuclear Overhauser effect spectroscopy). (*d*) Close-up view of the groove bound to the signal peptide. Green and red surfaces indicate, respectively, hydrophobic and acidic residues. The peptide is shown as a ribbon ball-and-stick representation, and most of its residues are numbered. The structural data reveal a dual binding mode for the peptide, which is capable of using both its positively charged N terminus and the α-helical hydrophobic region to interact with the same groove in SecA. Modified from Reference 49 with permission.

Over 160 intermolecular distance restraints were used to determine the structure of the complex, and it provided the first insight into the structural basis for signal-sequence recognition by SecA.

The recognition of signal sequences by receptors, such as SecA, controls the entry of proteins to export pathways (50, 55). For the translocase machinery to correctly sort secretory from nonsecretory proteins, the specific interaction between the signal sequence and SecA is a prerequisite (8). Thus, this binding interaction must be of extreme fidelity. SecA has the intriguing capacity to recognize hundreds of different signal sequences that nonetheless lack any consensus in their primary sequence (80). The only property that the signal sequences share is a stretch of hydrophobic residues preceded by positively charged residues in the N terminus. The NMR structure of the SecA–signal peptide complex (14) provided details of the recognition mode and the conformational changes that SecA undergoes to accommodate the signal sequence. Biochemical experiments motivated by the structural data showed that the signal sequence acts as an allosteric activator of the translocase (16).

THE NUCLEOSOME–HMGN2 COMPLEX

The packaging of the eukaryotic genome into chromatin is regulated by the interaction of nucleosomes with various proteins, such as chromatic factors and enzymes (5, 67). Despite the key role of these complexes, the structural basis for their formation is poorly understood. The HMGN protein, via its binding to the nucleosome, plays important parts in various processes, including transcription, DNA repair, chromatin remodeling, and histone modification (20, 67). The intrinsically disordered conformation of HMGN has hindered structural characterization of its complex with the nucleosome. Yawen Bai's lab (30) applied methyl TROSY NMR experiments to gain insights into the binding mechanism of the HMGN2 protein and the 230-kDa nucleosome core particle (NCP). The NCP contains two copies of each of the four histone proteins (H2A, H2B, H3, and H4) that are encircled by a long stretch of double-stranded DNA (**Figure 3*a***). Because the nucleosome can be reconstituted in vitro from its four histones, a number of samples were prepared wherein only one histone at a time was labeled in ILV (Ile, Leu, Val) methyl groups (**Figure 3*b***). This approach resulted in simplification of the methyl spectra. Earlier applications of methyl TROSY in large proteins, such as proteasomes (64) and the SecA ATPase (14), benefited from a divide and conquer approach to assigning the methyl resonances. Because this approach was not applicable to the NCP, the authors prepared a large number of mutations, which together with NOESY data, yielded the assignment for approximately 90% of the histone ILV methyl groups.

The binding site in the NCP for HMGN2 was initially identified by CSP analysis, and the data were further corroborated by saturation transfer experiments. The identified binding interface was further verified by mutagenesis studies. The NMR titration results were fitted to various models, revealing the cooperative binding of two HMGN2 molecules to one NCP, with additional weak, nonspecific binding to DNA. Next, PRE experiments were performed to obtain intermolecular distance restraints between HMGN2 and the NCP (**Figure 3*c***). Using both CSP and PRE data as restraints, the complex between NCP and HMGN2 was determined using the HADDOCK docking program (high ambiguity driven protein–protein docking) (12). The structural data revealed that HMGN2 bound to both the acidic patch in the H2A–H2B histone dimer and to nucleosomal DNA, thus stapling the histone core and the DNA (**Figure 3*d***). The nucleosome binding domain of HMGN2 binds to the NCP in an extended form. These structural data explain earlier observations that HMGN2 binding stabilizes the nucleosome and also how HMGNs are released during mitosis from chromatin upon phosphorylation of Ser residues that are involved in mediating complex formation. The HMGN2–nucleosome complex is mediated primarily by electrostatic contacts, which explains how HMGN2 can bind strongly to chromatin

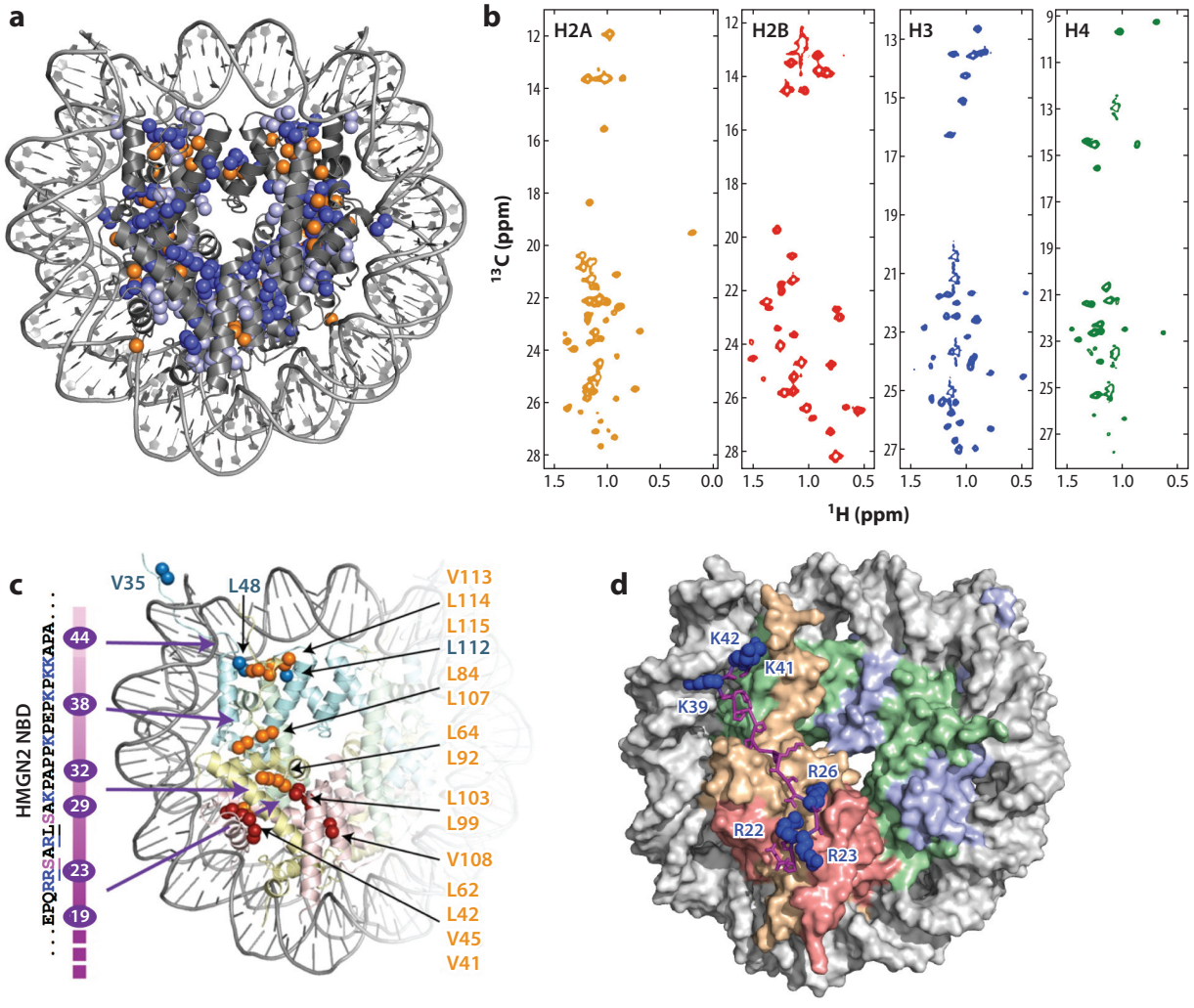

Figure 3

Nuclear magnetic resonance (NMR) structure determination of the complex between the nucleosome and HMGN2 (high mobility group nucleosomal 2). (*a*) Distribution of ILV (Ile, Leu, Val) methyl groups in the nucleosome structure. The backbone of the histones is shown with ribbons; ILV methyl groups are shown as spheres. Ile is orange, Leu is dark blue, and Val is light blue. (*b*) Methyl TROSY (transverse relaxation optimized spectroscopy) spectra of ILV methyl-bearing H2A, H2B, H3, and H4 in the nucleosome. Each histone was individually labeled by in vitro reconstitution of the nucleosome particle. (*c*) Summary of structural information derived from NMR chemical shift perturbation and paramagnetic spin labeling experiments. Methyl groups with large chemical shift changes or decreases in peak intensity upon binding to HMGN2 protein are labeled. Color coding for each histone is as shown in panel *b*. The sequence of the nucleosome binding domain of HMGN2 and the position of the spin labels are shown on the left. Arg and Lys residues, whose involvement in binding has been verified by mutagenesis, are highlighted in blue, and Ser24 and Ser28, which undergo phosphorylation during mitosis, are shown in magenta. (*d*) The docking structure of the nucleosome binding domain (NBD)–nucleosome complex. The NBD of HMGN2 is shown with sticks, and the side chains of the positively charged residues are indicated with blue balls. The nucleosome is presented as a solvent-exposed surface. Panels *b–d* reproduced with permission from Reference 29, copyright 2011, National Academy of Sciences, USA.

while be transiently associated with each single site. The overall architecture of the complex also suggests a general mechanism for regulating the structure and function of chromatin by HMGNs.

THE ClpB–DnaK COMPLEX

Molecular chaperones maintain a functional proteome in the cell by preventing the aggregation of unfolded proteins, assisting with their folding, or disassembling aggregates (7, 33). The heat-shock protein ClpB (or Hsp100) is the major protein disaggregase in bacteria, yeast, and the mitochondria of all eukaryotic cells, and it is essential for cell survival during severe stress (82). ClpB is an AAA+ (ATPases associated with various cellular activities), and ATP hydrolysis is required for its protein disaggregase action (51). However, recovering and resolubilizing proteins in their functional form from aggregates necessitate the synergistic action of ClpB with the Hsp70 (DnaK) chaperone (18). Despite the central role of this bichaperone system in protein disaggregation, its underlying mechanisms of function are poorly understood. Structural characterization of the ClpB–DnaK complex has been hindered by the weak interaction of the two proteins, as well as by their dynamic nature.

In a seminal contribution, the lab of Lewis Kay (57) used methyl TROSY NMR approaches to investigate the binding mechanism between the 580-kDa ClpB hexamer and the 70-kDa DnaK (**Figure 4*a*,*b***). The binding surface for each of the proteins was identified by a series of NMR titrations using selectively methyl-labeled samples (**Figure 4*c*,*d***). By fitting the chemical-shift changes, the dissociation constant (K_d) of the complex was measured to be approximately 25 μM, confirming the weak affinity of the complex. CSP mapping, together with biochemical experiments, established that the coiled-coil domain of ClpB and the N-terminal nucleotide binding domain of DnaK mediate complex formation. Because the structures of ClpB and DnaK in their free state were known, the authors sought to measure the intermolecular distance restraints to determine the structure of the complex. A spin label was introduced in ClpB in various positions (one at a time) and the PRE rates of the DnaK methyls were measured. The long-range distance constraints, together with the binding interface identified by CSP data, were fed into the HADDOCK program, and the docked ClpB–DnaK complex was obtained (**Figure 4*e***). Interestingly, the binding site of ClpB on DnaK was found to overlap that of the cochaperone GrpE, whose binding to DnaK leads to nucleotide dissociation and subsequent substrate release (17). This observation was further corroborated by a set of competition experiments. Biochemical assays showed that GrpE appears to have a deleterious effect on the disaggregation reaction (61). Of note, it was found that ClpB can release aggregated substrates from DnaK and the interaction between DnaK and ClpB activates the process. A plausible mechanistic model for the aggregated protein reactivation by ClpB was put forward (**Figure 4*f***) (61). The study provided atomic insight into the assembly of the bichaperone ClpB–DnaK system and revealed key steps in the protein disaggregation process.

THE BOX C/D RIBONUCLEOPROTEIN ENZYME COMPLEX

Posttranscriptional modification of 2′-*O*-ribose methylation in eukaryotes and archaea is catalyzed by an enzyme called the box C/D small nucleolar RNA protein complex. During this process, the box C/D ribonucleoprotein (RNP) complex uses a multitude of guide RNAs as templates to recognize ribosomal RNA target sites and subsequently carries out methylation of ribosomal RNA at the 2′-*O*-ribose (38). The archaeal counterpart box C/D enzyme complex consists of three core proteins—L7Ae, Nop5, and fibrillarin—and a 72-base guide small RNA. Overwhelming evidence has shown that fibrillarin is the catalytic subunit responsible for the methyl transfer reaction (2). However, the detailed catalytic mechanism remains poorly understood. Moreover, the significance of two methylation guide sequences on each guide RNA remains unclear.

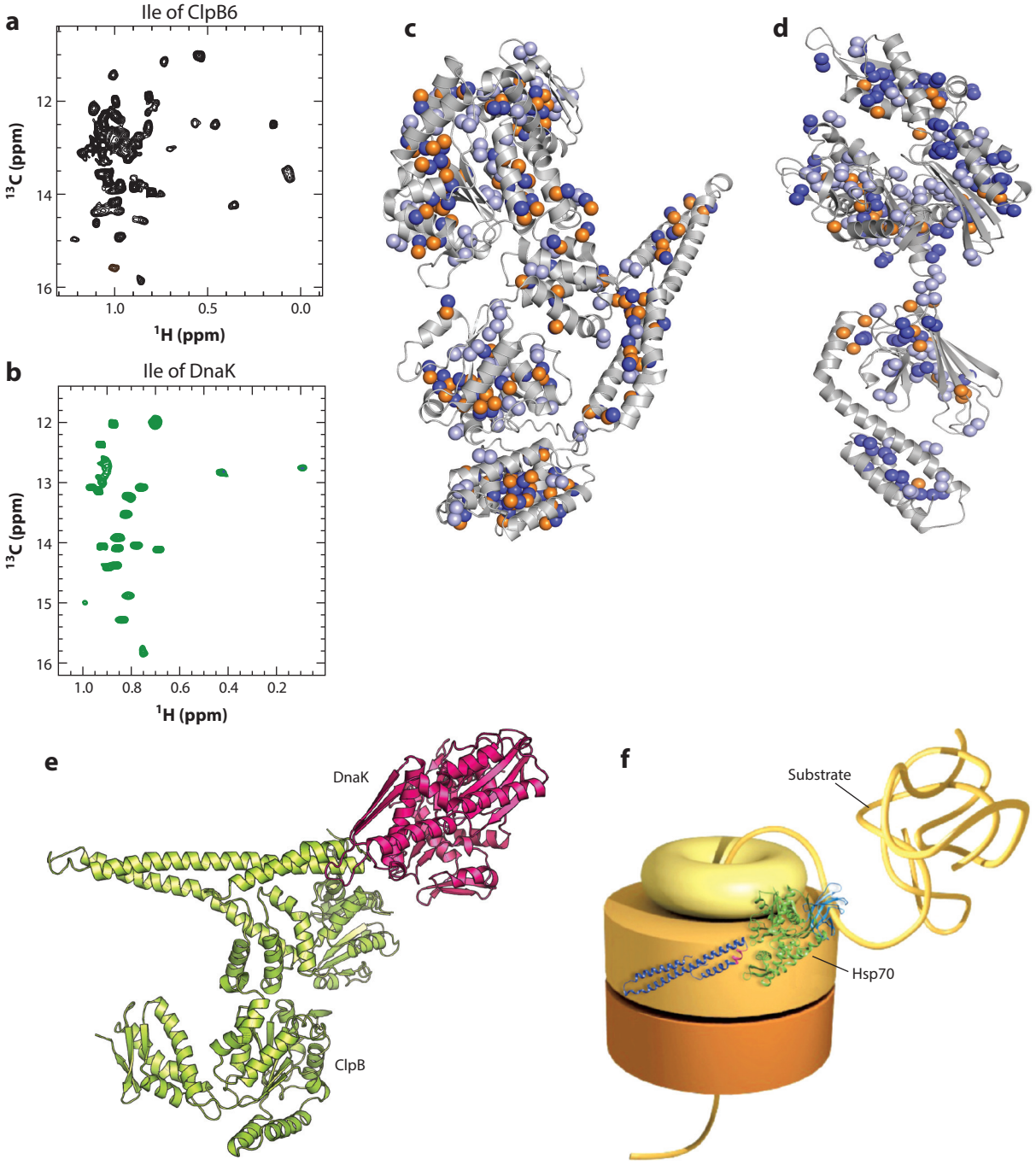
a
Ile of ClpB6
^{13}C (ppm)
12
14
16
1.0
0.5
0.0
^{1}H (ppm)
b
Ile of DnaK
^{13}C (ppm)
12
13
14
15
16
1.0
0.8
0.6
0.4
0.2
^{1}H (ppm)
c
d
e
DnaK
ClpB
f
Substrate
Hsp70

To characterize the architecture and illuminate the mechanism of the box C/D RNP enzyme, Teresa Carlomagno's lab (35) used solution NMR in combination with small-angle neutron scattering (SANS) to determine the structural assembly of both the apo and holo (conjugated) forms of the 390-kDa archaeal RNP enzyme. Methyl TROSY experiments were carried out to monitor CSPs of methyl ILV-labeled fibrillarin and L7Ae upon stepwise formation of the complex (**Figure 5*a***). The results, together with PRE-derived distance restraints (**Figure 5*b***), confirmed that the binding interfaces of the protein subunits in the full enzyme complex are essentially identical to those previously observed in the crystal structures of enzyme segments. Moreover, combining the intermolecular long-distance restraints derived from PRE experiments with the small-angle neutron-scattering data (SANS), which define the shape of each component in the context of the full complex, allowed the authors to determine the structure of the RNP enzyme in the apo form (**Figure 5*c***) and bound to RNA substrate (**Figure 5*d***). Notably, the enzyme undergoes a drastic structural rearrangement upon substrate binding. Interestingly, a small set of PRE data obtained from the apo form of the RNP enzyme fits well within the structure of the holo form, suggesting that the apo RNP complex exists in dynamic equilibrium between a pair of alternate conformations in solution. Based on this observation, the authors put forward an occasional fly casting–motion model for the catalytic module fibrillarin. According to this model, the catalytic fibrillarin may visit the space close to the small RNA in the apo complex, and it likely aids in the recognition of the guide–substrate duplex. In addition, the binding of the substrate RNA causes a few resonances of the fibrillarin subunit to split into two peaks, with one set corresponding to the apo form, and the two sets of peaks reached plateaus of the same intensity. This finding argues that only two of the four fibrillarin copies are in contact with the substrate RNAs in the holo complex, whereas the other two copies are in the same environment as in the apo complex. This tour de force study provided structural and mechanistic insights for a model of a sequential methylation mechanism with differential control of methylation levels at the two sites; at the same time, it offers an unexpected regulatory mechanism for ribosomal RNA folding (35).

THE TRIGGER FACTOR–PhoA COMPLEX

Molecular chaperones recognize and bind to solvent-exposed hydrophobic segments of non-native proteins, thereby preventing these proteins from aggregating or misfolding. Despite the central importance of the interaction of non-native proteins with chaperones, the structural basis of the complex formation has remained poorly understood. The scarcity of structural data about

Figure 4

Nuclear magnetic resonance (NMR) structure determination of the complex between ClpB and DnaK. (*a*) Methyl TROSY (transverse relaxation optimized spectroscopy) spectrum of the Ile region of the ClpB hexamer (580 kDa). (*b*) Methyl TROSY spectrum of the Ile region of DnaK. (*c*,*d*) Ile, Leu, and Val methyl group distribution in (*c*) *Thermus thermophilus* ClpB and (*d*) *T. thermophilus* DnaK. The structural model for *T. thermophilus* DnaK was generated using the SWISS-MODEL website (Biozentrum, University of Basel; **https://swissmodel.expasy.org/**) and based on sequence homology with the crystal structure 2KHO in the Protein Data Bank. Ile methyl groups are shown as orange spheres, and the methyl groups of Leu and Val are shown as, respectively, dark blue and light blue spheres. (*e*) Structure of ClpB (*yellow*) in complex with DnaK (*pink*). Because they are not involved in complex formation, the ClpB nucleotide binding domain 2 (NBD2) and the DnaK C-terminal substrate binding domain (SBD) are not shown. (*f*) Mechanistic model of collaboration between the ClpB and DnaK systems in the protein disaggregation process (61). The DnaK SBD (*light blue*) interacts with the aggregated protein substrate (*yellow string*) and recruits it through the pore channel of ClpB disaggregase (denoted by *three stacked rings*) via direct interaction of the DnaK NBD (*green*) with the coiled-coil domain of ClpB (*dark blue*). After translocation through the ClpB central pore, the released, unfolded polypeptides refold to their native state, either spontaneously or with the aid of refolding chaperones. Panel *f* reproduced with permission from Reference 61, copyright 2013, Nature Publishing Group.

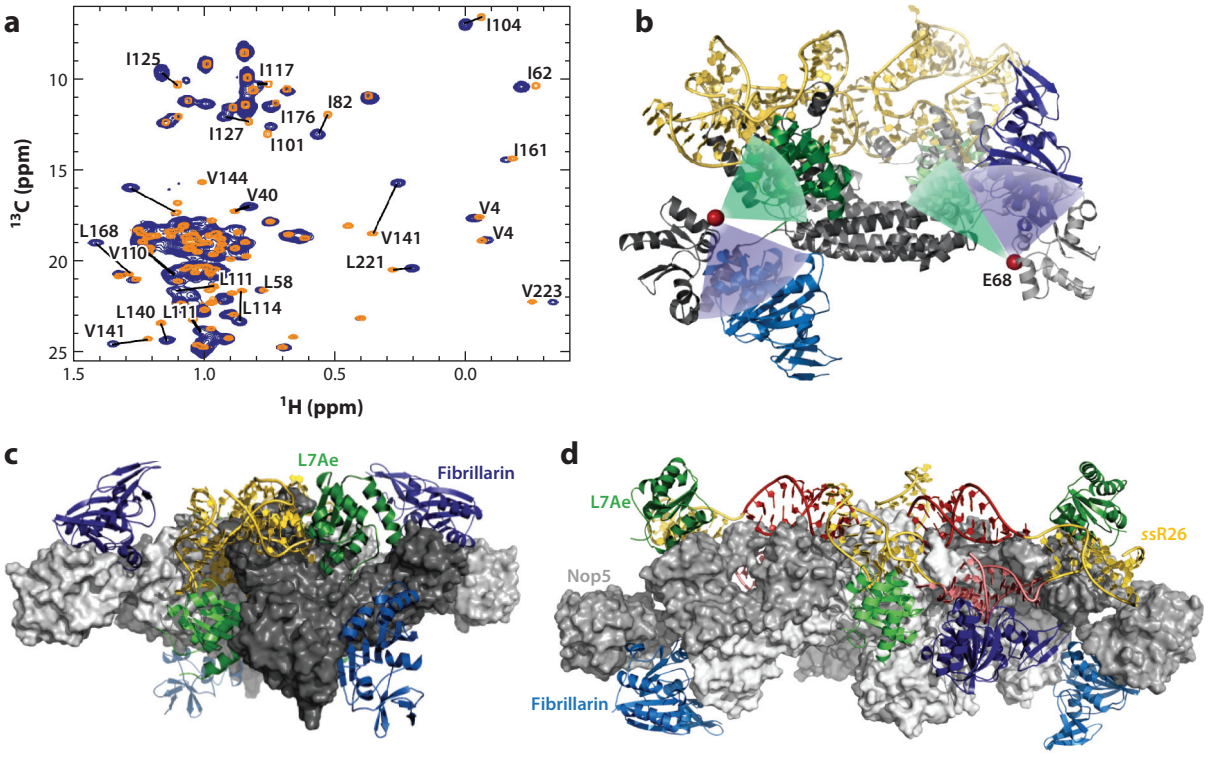

Figure 5

Determination of the structure of the box C/D ribonucleoprotein (RNP) enzyme complex by nuclear magnetic resonance (NMR) spectroscopy. (*a*) Verification of interaction interfaces in the subcomplexes. Overlay of the ^{1}H–^{13}C methyl TROSY of ILV (Ile, Leu, Val) methyl-labeled fibrillarin (*orange*) and in complex with unlabeled Nop5 (*blue*). The residues that experienced large chemical shift perturbations are labeled. Spectral analysis confirmed that the interaction surface between fibrillarin and Nop5 in the box C/D RNP is essentially identical to the one previously seen in the crystal structures of the Nop5–fibrillarin subcomplex. (*b*) PRE (paramagnetic relaxation enhancement) measurements used to obtain long-range distance restraints. The spin label at the E68 position (*red spheres*) on Nop5 is shown as an example, with the fibrillarin (*blue*) or L7Ae (*green*) funnels indicating the protein for which PRE effects were measured. (*c*) Structure of the apo (nucleotide free) box C/D sRNP (small ribonucleoprotein) determined by NMR and data from small-angle neutron scattering. The subunits within the complex are denoted using different colors. The Nop5 copies, which form a platform, are shown as a gray surface. The other complex elements are shown in a schematic using different colors. (*d*) Structure of the holo (conjugated) RNP (subunit colors as in *b*). Note that when compared with panel *c*, large conformational changes occur upon substrate binding. In this structure, only two fibrillarin copies (*dark blue*) contact the guide–substrate D′ duplexes (*salmon*) and are able to perform methylation; the other two copies (*light blue*) are in the off position, opposite the corresponding guide–substrate D duplexes (*red*). This structure, together with a further NMR-based enzyme-activity assay, allowed the authors to propose a sequential methylation mechanism. Reproduced with permission from Reference 35, copyright 2013, Nature Publishing Group.

complexes formed between chaperones and non-native proteins is primarily due to the technical challenges originating in the size and dynamic nature of these complexes. Our lab (62) exploited recent advances in NMR and isotope-labeling approaches to characterize the dynamic binding of unfolded alkaline phosphatase (PhoA) to the TF chaperone and to determine the solution structure of PhoA captured in an extended, unfolded state by three TF molecules.

Bacterial TF binds to the exit channel of the ribosome and directly interacts with the emerging nascent polypeptide (13). Because of TF's high cellular concentration (approximately 50 μM), about half of TF molecules are ribosome free and function as generalized molecular chaperones in the cytosol (76). Deletion of the *TF* gene results in the aggregation of many proteins and as

a defense mechanism the heat-shock response is stimulated (15, 48). Multiple TF molecules are required to engage long polypeptides (>20 kDa), which are the preferred clients for TF in vivo (25, 48). Because the primary goal of the study by Saio et al. (62) was to determine the high-resolution structure of the TF–PhoA complex, they developed protocols to increase proton density, which was achieved by simultaneously labeling all sizes of methyl-bearing (Ala, Ile, Met, Leu, Thr, and Val) and aromatic (Phe, Trp, and Tyr) residues (**Figure 6*a***). The NMR spectra of TF were of high quality (**Figure 6*b***). PhoA (471 amino acids) was used as an unfolded substrate because of its unique feature of unfolding under reducing conditions without the need for chaotropic agents, and the fact that it remains monodisperse and well dispersed in its unfolded state. A series of NMR titrations revealed seven distinct TF binding regions in PhoA molecules, enriched both in hydrophobic and, especially, in aromatic residues, and four substrate binding sites on TF (**Figure 6*c***).

A combined NMR, light-scattering and isothermal titration calorimetry approach showed that three TF molecules are needed to engage all seven binding sites of PhoA, thus forming a 200 kDa complex in solution. A thorough NMR analysis then defined the exact PhoA regions that formed the most stable complex with each TF molecule. This resulted in homogeneous samples of TF–PhoA complexes and, thus, high-quality NMR spectra of these complexes. Assisted by a powerful combinatorial labeling scheme, hundreds of intermolecular NOEs were collected for the TF–PhoA complexes. Used together with a large number of intra-TF NOEs, this strategy yielded the de novo high-resolution structure of each one of the three TF–PhoA complexes in the 200 kDa TF–PhoA assembly (**Figure 6*d***). These were the first high-resolution structures determined for a molecular chaperone in complex with an unfolded protein. The structural data revealed there was a multivalent binding mechanism between the chaperone and its protein substrate. This mechanism of binding presents several advantages as it enables chaperones to function as holdases and unfoldases by exerting forces to retain proteins in the unfolded state and at the same time protect them from aggregation by shielding their exposed hydrophobic regions. The structural data of the three TF molecules in complex with different regions of PhoA revealed how the same binding sites within a molecular chaperone can recognize and interact with a large number of substrates that have unrelated primary sequences. This promiscuous recognition is further enabled by the notable plasticity of the substrate binding sites in TF.

THE SecB–PhoA COMPLEX

Molecular chaperones exert their functions by recognizing and interacting with exposed hydrophobic segments in non-native proteins. Despite common features, different families of chaperones exhibit distinct activity and biological function (42). Chaperones may exhibit foldase activity, whereby they accelerate the folding of client proteins, or antifolding (holdase) activity, whereby they delay the folding of client proteins, and the strength of the activity can vary significantly (33). Molecular chaperones come in different sizes and a great variety of shapes (60). However, the scarcity of structural data about chaperones in complex with non-native proteins has impeded the understanding of how different chaperones engage these proteins and how distinct chaperone architectures may alter activity.

To understand how the architecture of a chaperone affects its activity, our lab (21) characterized SecB, a cytosolic chaperone that exhibits an unusually strong antifolding activity (63). SecB has at least two distinct roles in the cell: (*a*) It is responsible for maintaining secretory proteins in an unfolded, secretion-competent state, followed by targeting their delivery to the SecA ATPase (4); and (*b*) it also has a role as a generalized chaperone to prevent protein misfolding and aggregation (77). SecB exists as a tetramer (approximately 70 kDa) organized as a dimer of dimers, with an overall rectangular, disk-like shape (83). The NMR spectra of SecB labeled in methyl-bearing

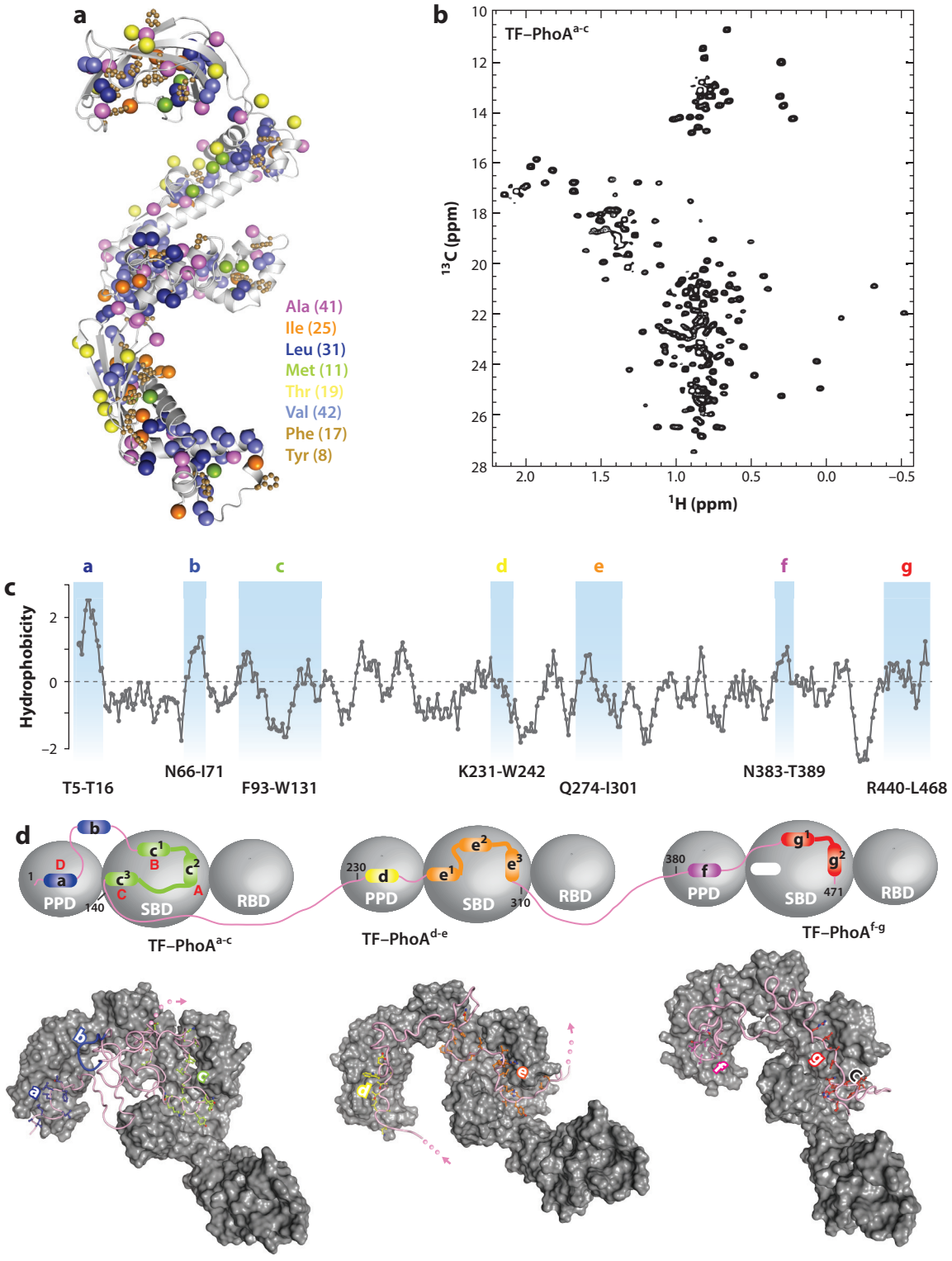
a
Ala (41)
Ile (25)
Leu (31)
Met (11)
Thr (19)
Val (42)
Phe (17)
Tyr (8)
b
TF–PhoA^a-c
13C (ppm)
1H (ppm)
c
Hydrophobicity
a
b
c
d
e
f
g
T5-T16
N66-I71
F93-W131
K231-W242
Q274-I301
N383-T389
R440-L468
d
PPD
SBD
RBD
TF–PhoA^a-c
TF–PhoA^d-e
TF–PhoA^f-g

(Ala, Ile, Met, Leu, Thr, and Val) and aromatic (Phe, Trp, and Tyr) residues (**Figure 7*a***) are of high quality (**Figure 7*b***), and near-complete assignment has been obtained. Both maltose binding protein (MBP) and PhoA were used as protein substrates for SecB. NMR analysis showed that there are five distinct SecB recognition sites in PhoA (**Figure 7*c***) and seven sites in MBP, with all sites being enriched in hydrophobic and aromatic residues. To determine the client binding sites in SecB, Huang et al. (21) identified the SecB residues that showed intermolecular NOEs to short fragments of PhoA- and MBP-encompassing SecB recognition sites. The SecB residues that interact with the substrates collectively form long, continuous hydrophobic grooves that constitute the primary binding sites for non-native proteins. NMR-monitored refolding experiments of protein substrates demonstrated that, indeed, SecB can retain bound proteins in an unfolded state for prolonged periods.

SecB forms a stoichiometric complex of 120 kDa with PhoA. Using a number of selectively labeled methyl and aromatic samples in a combinatorial labeling scheme, more than 200 intermolecular NOEs were determined for the SecB–PhoA complex. The resulting structure of the complex and the overall positioning of PhoA on SecB were further validated by PRE experiments. The most remarkable feature is that PhoA wraps around SecB in an overall arrangement that maximizes the interacting surface between the client protein, which is held in an unfolded conformation, and the chaperone (**Figure 7*d***). The simultaneous engagement of all PhoA sites by SecB results in significant enhancement of the affinity of the unfolded protein for SecB. However, the binding synergy is not strong, probably because the linkers tethering the SecB recognition sites in PhoA are long and flexible. Analysis of the SecB–PhoA structure revealed how SecB recognizes PhoA and how it accommodates all five PhoA sites within one SecB molecule. Interestingly, the primary binding grooves in SecB expand to accommodate the large nonpolar side chains of the client. Thus, SecB can adjust the structure of the primary binding grooves to allow longer substrates to fit into the groove.

The structural data, together with kinetic and thermodynamic data, demonstrate how the distinctive binding mode of SecB for non-native proteins enables the chaperone to prevent the folding of bound proteins (**Figure 7*e***). Compared with TF, the structural data explain how the overall architecture of the chaperone and the way it engages non-native proteins give rise to different chaperone activities. Because SecB recognizes and binds to multiple regions within an unfolded protein, long client proteins wrap around SecB to maximize the binding interface, thereby altering the binding kinetics. The overall binding architecture appears to be unique among known protein–protein complexes.

Figure 6

Nuclear magnetic resonance (NMR) determination of the structure of the TF–PhoA (trigger factor–alkaline phosphatase) complex. (*a*) TF is enriched in hydrophobic residues, such as methyl-bearing (Ala, Ile, Leu, Met, Thr, and Val) and aromatic residues (Phe and Tyr). The numbers in parentheses indicate the number of corresponding residues in TF (per subunit). (*b*) ^{1}H-^{13}C methyl TROSY (transverse relaxation optimized spectroscopy) spectra of [U-^{2}H; Ala-$^{13}CH_3$; Met-$^{13}CH_3$; Ile-δ1-$^{13}CH_3$; Leu,Val-$^{13}CH_3$/$^{12}CD_3$]-labeled TF–PhoA^{a-c} complex. (*c*) Plot of the hydrophobicity of PhoA as a function of its primary sequence. A hydrophobicity score (Roseman algorithm, window = 9) higher than zero denotes increased hydrophobicity. The seven PhoA regions (labeled *a* through *g*) identified by NMR as interacting with TF are highlighted (*light blue*). The residue range of the sites is shown on the left. (*d*, *top*) Schematic of the interaction of PhoA with TF based on current structural data. (*Bottom*) The TF binding sites in PhoA. Lowest-energy structure of the three TF molecules in complex with the corresponding PhoA regions. TF is shown as a solvent-exposed surface and PhoA as a pink ribbon. The PhoA residues that directly interact with TF are drawn in a ball-and-stick representation. The pink arrows denote the direction of the PhoA chain, from the N to the C terminus. Abbreviations: PPD, peptidyl prolyl isomerase domain; RBD, ribosome binding domain; SBD, substrate binding domain. Modified from Reference 62 with permission, copyright 2014, American Association for the Advancement of Science.

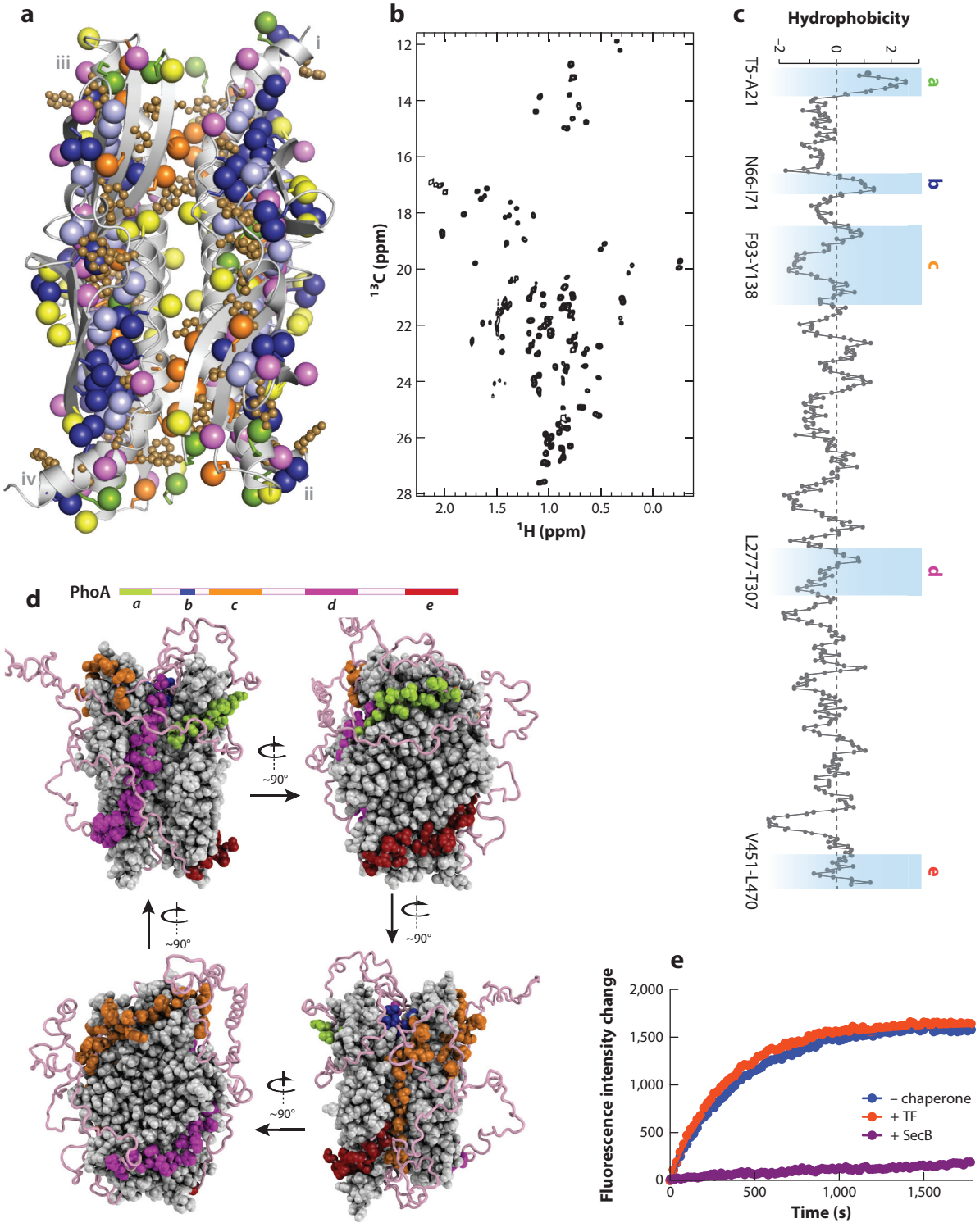
a
i
ii
iii
iv
b
^{13}C (ppm)
^{1}H (ppm)
c
Hydrophobicity
T5-A21
N66-I71
F93-Y138
L277-T307
V451-L470
a
b
c
d
e
d
PhoA
a
b
c
d
e
~90°
~90°
~90°
~90°
e
Fluorescence intensity change
Time (s)
– chaperone
+ TF
+ SecB

Figure 7

Nuclear magnetic resonance (NMR) determination of the structure of SecB–PhoA (alkaline phosphatase) complex. (*a*) SecB is enriched in hydrophobic amino acids, such as methyl-bearing (Ala, Ile, Leu, Met, Thr, and Val) and aromatic (Phe and Tyr) residues. Leu, dark blue spheres; Val, light blue spheres; Ile, orange spheres; Met, yellow spheres; Thr, green spheres, Phe and Tyr, brown spheres. The four subunits are labeled *i* through *iv*. (*b*) ^{1}H–^{13}C methyl TROSY (transverse relaxation optimized spectroscopy) spectrum of [U-^{2}H; Ala-$^{13}CH_3$; Met-$^{13}CH_3$; Ile-δ1-$^{13}CH_3$; Leu,Val-$^{13}CH_3$/$^{13}CH_3$; Thr-$^{13}CH_3$]-labeled SecB. SecB packing gives rise to two pairs of spectroscopically equivalent subunits: One pair is formed by subunits *i* and *iv* in panel *a*, and the other pair by subunits *ii* and *iii* in panel *a*. (*c*) Plot of the hydrophobicity of PhoA as a function of its primary sequence. A hydrophobicity score (Roseman algorithm, window = 9) higher than zero denotes increased hydrophobicity. The sites identified by NMR as being recognized by SecB in PhoA (labeled *a–e*) are highlighted in blue and the residue range is shown on the left. (*d*) Lowest-energy structure of the SecB–PhoA complex. SecB is shown as a space-filling model in gray. The five PhoA sites recognized by SecB are shown as space-filling models and colored as in the schematic of the PhoA sequence at the top. The flexible regions of PhoA are shown as a pink ribbon. Four views of the complex are shown related by a rotation as indicated by the arrow. One PhoA molecule binds and this wraps around SecB. The NMR data show that the linkers tethering the binding sites in PhoA are flexible and do not interact with SecB. (*e*) Folding of urea-denatured maltose binding protein in the absence of a chaperone (*blue*) and in the presence of SecB (*purple*) or TF (*orange*). SecB prevents the folding of MBP, whereas TF has a negligible effect. Reproduced with permission from Reference 21, copyright 2016, Nature Publishing Group.

DISCLOSURE STATEMENT

The authors are not aware of any affiliations, memberships, funding, or financial holdings that might be perceived as affecting the objectivity of this review.

LITERATURE CITED

1. Ahnert SE, Marsh JA, Hernandez H, Robinson CV, Teichmann SA. 2015. Principles of assembly reveal a periodic table of protein complexes. *Science* 350:aaa2245
2. Aittaleb M, Rashid R, Chen Q, Palmer JR, Daniels CJ, Li H. 2003. Structure and function of archaeal box C/D sRNP core proteins. *Nat. Struct. Mol. Biol.* 10:256–63
3. Ali MM, Roe SM, Vaughan CK, Meyer P, Panaretou B, et al. 2006. Crystal structure of an Hsp90–nucleotide–p23/Sba1 closed chaperone complex. *Nature* 440:1013–17
4. Bechtluft P, Nouwen N, Tans SJ, Driessen AJ. 2010. SecB—a chaperone dedicated to protein translocation. *Mol. Biosyst.* 6:620–27
5. Becker PB, Horz W. 2002. ATP-dependent nucleosome remodeling. *Annu. Rev. Biochem.* 71:247–73
6. Boehr DD, Nussinov R, Wright PE. 2009. The role of dynamic conformational ensembles in biomolecular recognition. *Nat. Chem. Biol.* 5:789–96
7. Bukau B, Weissman J, Horwich A. 2006. Molecular chaperones and protein quality control. *Cell* 125:443–51
8. Chatzi KE, Sardis MF, Economou A, Karamanou S. 2014. SecA-mediated targeting and translocation of secretory proteins. *Biochim. Biophys. Acta* 1843:1466–74
9. Chen L, Balabanidou V, Remeta DP, Minetti CA, Portaliou AG, et al. 2011. Structural instability tuning as a regulatory mechanism in protein–protein interactions. *Mol. Cell* 44:734–44
10. Clore GM. 2015. Practical aspects of paramagnetic relaxation enhancement in biological macromolecules. *Methods Enzymol.* 564:485–97
11. Dollins DE, Warren JJ, Immormino RM, Gewirth DT. 2007. Structures of GRP94–nucleotide complexes reveal mechanistic differences between the hsp90 chaperones. *Mol. Cell* 28:41–56
12. Dominguez C, Boelens R, Bonvin AM. 2003. HADDOCK: a protein–protein docking approach based on biochemical or biophysical information. *J. Am. Chem. Soc.* 125:1731–37
13. Ferbitz L, Maier T, Patzelt H, Bukau B, Deuerling E, Ban N. 2004. Trigger factor in complex with the ribosome forms a molecular cradle for nascent proteins. *Nature* 431:590–96
14. Gelis I, Bonvin AM, Keramisanou D, Koukaki M, Gouridis G, et al. 2007. Structural basis for signal-sequence recognition by the translocase motor SecA as determined by NMR. *Cell* 131:756–69

15. Genevaux P, Keppel F, Schwager F, Langendijk-Genevaux PS, Hartl FU, Georgopoulos C. 2004. In vivo analysis of the overlapping functions of DnaK and trigger factor. *EMBO Rep*. 5:195–200
16. Gouridis G, Karamanou S, Gelis I, Kalodimos CG, Economou A. 2009. Signal peptides are allosteric activators of the protein translocase. *Nature* 462:363–67
17. Harrison CJ, Hayer-Hartl M, Di Liberto M, Hartl F, Kuriyan J. 1997. Crystal structure of the nucleotide exchange factor GrpE bound to the ATPase domain of the molecular chaperone DnaK. *Science* 276:431–35
18. Haslberger T, Zdanowicz A, Brand I, Kirstein J, Turgay K, et al. 2008. Protein disaggregation by the AAA+ chaperone ClpB involves partial threading of looped polypeptide segments. *Nat. Struct. Mol. Biol.* 15:641–50
19. Hiller S, Wagner G. 2009. The role of solution NMR in the structure determinations of VDAC-1 and other membrane proteins. *Curr. Opin. Struct. Biol.* 19:396–401
20. Hock R, Furusawa T, Ueda T, Bustin M. 2007. HMG chromosomal proteins in development and disease. *Trends Cell Biol*. 17:72–79
21. Huang C, Rossi P, Saio T, Kalodimos CG. 2016. Structural basis for the antifolding activity of a molecular chaperone. *Nature* 537:202–6
22. Imai S, Osawa M, Takeuchi K, Shimada I. 2010. Structural basis underlying the dual gate properties of KcsA. *PNAS* 107:6216–21
23. Ittner LM, Ke YD, Delerue F, Bi M, Gladbach A, et al. 2010. Dendritic function of tau mediates amyloid-β toxicity in Alzheimer's disease mouse models. *Cell* 142:387–97
24. Kainosho M, Torizawa T, Iwashita Y, Terauchi T, Mei Ono A, Güntert P. 2006. Optimal isotope labelling for NMR protein structure determinations. *Nature* 440:52–57
25. Kaiser CM, Chang HC, Agashe VR, Lakshmipathy SK, Etchells SA, et al. 2006. Real-time observation of trigger factor function on translating ribosomes. *Nature* 444:455–60
26. Kalodimos CG. 2012. Protein function and allostery: a dynamic relationship. *Ann. N.Y. Acad. Sci.* 1260:81–86
27. Karagöz GE, Duarte AM, Akoury E, Ippel H, Biernat J, et al. 2014. Hsp90–Tau complex reveals molecular basis for specificity in chaperone action. *Cell* 156:963–74
28. Karagöz GE, Duarte AM, Ippel H, Uetrecht C, Sinnige T, et al. 2011. N-terminal domain of human Hsp90 triggers binding to the cochaperone p23. *PNAS* 108:580–85
29. Kasinath V, Valentine KG, Wand AJ. 2013. A ^{13}C labeling strategy reveals a range of aromatic side chain motion in calmodulin. *J. Am. Chem. Soc.* 135:9560–63
30. Kato H, van Ingen H, Zhou BR, Feng H, Bustin M, et al. 2011. Architecture of the high mobility group nucleosomal protein 2–nucleosome complex as revealed by methyl-based NMR. *PNAS* 108:12283–88
31. Kay LE. 2011. Solution NMR spectroscopy of supra-molecular systems, why bother? A methyl-TROSY view. *J. Magn. Reson.* 210:159–70
32. Kerfah R, Plevin MJ, Sounier R, Gans P, Boisbouvier J. 2015. Methyl-specific isotopic labeling: a molecular tool box for solution NMR studies of large proteins. *Curr. Opin. Struct. Biol.* 32:113–22
33. Kim YE, Hipp MS, Bracher A, Hayer-Hartl M, Hartl FU. 2013. Molecular chaperone functions in protein folding and proteostasis. *Annu. Rev. Biochem.* 82:323–55
34. Krukenberg KA, Forster F, Rice LM, Sali A, Agard DA. 2008. Multiple conformations of *E. coli* Hsp90 in solution: insights into the conformational dynamics of Hsp90. *Structure* 16:755–65
35. Lapinaite A, Simon B, Skjaerven L, Rakwalska-Bange M, Gabel F, Carlomagno T. 2013. The structure of the box C/D enzyme reveals regulation of RNA methylation. *Nature* 502:519–23
36. Latham MP, Sekhar A, Kay LE. 2014. Understanding the mechanism of proteasome 20S core particle gating. *PNAS* 111:5532–37
37. Li J, Buchner J. 2013. Structure, function and regulation of the Hsp90 machinery. *Biomed. J.* 36:106–17
38. Lin J, Lai S, Jia R, Xu A, Zhang L, et al. 2011. Structural basis for site-specific ribose methylation by box C/D RNA protein complexes. *Nature* 469:559–63
39. Ma C, Li W, Xu Y, Rizo J. 2011. Munc13 mediates the transition from the closed syntaxin–Munc18 complex to the SNARE complex. *Nat. Struct. Mol. Biol.* 18:542–49
40. Marsh JA, Teichmann SA. 2015. Structure, dynamics, assembly, and evolution of protein complexes. *Annu. Rev. Biochem.* 84:551–75

41. Marsh JA, Teichmann SA, Forman-Kay JD. 2012. Probing the diverse landscape of protein flexibility and binding. *Curr. Opin. Struct. Biol.* 22:643–50
42. Mattoo RU, Goloubinoff P. 2014. Molecular chaperones are nanomachines that catalytically unfold misfolded and alternatively folded proteins. *Cell. Mol. Life Sci.* 71:3311–25
43. Milbradt AG, Arthanari H, Takeuchi K, Boeszoermenyi A, Hagn F, Wagner G. 2015. Increased resolution of aromatic cross peaks using alternate ^{13}C labeling and TROSY. *J. Biomol. NMR* 62:291–301
44. Mittag T, Kay LE, Forman-Kay JD. 2010. Protein dynamics and conformational disorder in molecular recognition. *J. Mol. Recognit.* 23:105–16
45. Monneau YR, Ishida Y, Rossi P, Saio T, Tzeng SR, et al. 2016. Exploiting *E. coli* auxotrophs for leucine, valine, and threonine specific methyl labeling of large proteins for NMR applications. *J. Biomol. NMR* 65:99–108
46. Mund M, Overbeck JH, Ullmann J, Sprangers R. 2013. LEGO-NMR spectroscopy: a method to visualize individual subunits in large heteromeric complexes. *Angew. Chem. Int. Ed. Engl.* 52:11401–5
47. Nooren IM, Thornton JM. 2003. Diversity of protein–protein interactions. *EMBO J.* 22:3486–92
48. Oh E, Becker AH, Sandikci A, Huber D, Chaba R, et al. 2011. Selective ribosome profiling reveals the cotranslational chaperone action of trigger factor in vivo. *Cell* 147:1295–308
49. Papanikolau Y, Papadovasilaki M, Ravelli RB, McCarthy AA, Cusack S, et al. 2007. Structure of dimeric SecA, the *Escherichia coli* preprotein translocase motor. *J. Mol. Biol.* 366:1545–57
50. Papanikou E, Karamanou S, Economou A. 2007. Bacterial protein secretion through the translocase nanomachine. *Nat. Rev. Microbiol.* 5:839–51
51. Parsell DA, Kowal AS, Singer MA, Lindquist S. 1994. Protein disaggregation mediated by heat-shock protein Hsp104. *Nature* 372:475–78
52. Pearl LH. 2016. The HSP90 molecular chaperone—an enigmatic ATPase. *Biopolymers* 105:594–607
53. Pearl LH, Prodromou C. 2006. Structure and mechanism of the Hsp90 molecular chaperone machinery. *Annu. Rev. Biochem.* 75:271–94
54. Popovych N, Tzeng SR, Tonelli M, Ebright RH, Kalodimos CG. 2009. Structural basis for cAMP-mediated allosteric control of the catabolite activator protein. *PNAS* 106:6927–32
55. Rapoport TA. 2007. Protein translocation across the eukaryotic endoplasmic reticulum and bacterial plasma membranes. *Nature* 450:663–69
56. Rosenzweig R, Kay LE. 2014. Bringing dynamic molecular machines into focus by methyl-TROSY NMR. *Annu. Rev. Biochem.* 83:291–315
57. Rosenzweig R, Moradi S, Zarrine-Afsar A, Glover JR, Kay LE. 2013. Unraveling the mechanism of protein disaggregation through a ClpB–DnaK interaction. *Science* 339:1080–83
58. Ruschak AM, Religa TL, Breuer S, Witt S, Kay LE. 2010. The proteasome antechamber maintains substrates in an unfolded state. *Nature* 467:868–71
59. Russel D, Lasker K, Webb B, Velazquez-Muriel J, Tjioe E, et al. 2012. Putting the pieces together: integrative modeling platform software for structure determination of macromolecular assemblies. *PLOS Biol.* 10:e1001244
60. Saibil HR. 2008. Chaperone machines in action. *Curr. Opin. Struct. Biol.* 18:35–42
61. Saibil HR. 2013. Chaperone machines for protein folding, unfolding and disaggregation. *Nat. Rev Mol. Cell Biol.* 14:630–42
62. Saio T, Guan X, Rossi P, Economou A, Kalodimos CG. 2014. Structural basis for protein antiaggregation activity of the trigger factor chaperone. *Science* 344:1250494
63. Sala A, Bordes P, Genevaux P. 2014. Multitasking SecB chaperones in bacteria. *Front. Microbiol.* 5:666
64. Sprangers R, Kay LE. 2007. Quantitative dynamics and binding studies of the 20S proteasome by NMR. *Nature* 445:618–22
65. Street TO, Lavery LA, Agard DA. 2011. Substrate binding drives large-scale conformational changes in the Hsp90 molecular chaperone. *Mol. Cell* 42:96–105
66. Taipale M, Krykbaeva I, Koeva M, Kayatekin C, Westover KD, et al. 2012. Quantitative analysis of HSP90–client interactions reveals principles of substrate recognition. *Cell* 150:987–1001
67. Tan S, Davey CA. 2011. Nucleosome structural studies. *Curr. Opin. Struct. Biol.* 21:128–36
68. Teilum K, Brath U, Lundström P, Akke M. 2006. Biosynthetic ^{13}C labeling of aromatic side chains in proteins for NMR relaxation measurements. *J. Am. Chem. Soc.* 128:2506–7

69. Tompa P, Fuxreiter M. 2008. Fuzzy complexes: polymorphism and structural disorder in protein–protein interactions. *Trends Biochem. Sci.* 33:2–8
70. Tugarinov V, Choy WY, Orekhov VY, Kay LE. 2005. Solution NMR–derived global fold of a monomeric 82-kDa enzyme. *PNAS* 102:622–27
71. Tugarinov V, Kanelis V, Kay LE. 2006. Isotope labeling strategies for the study of high-molecular-weight proteins by solution NMR spectroscopy. *Nat. Protoc.* 1:749–54
72. Tzeng SR, Kalodimos CG. 2011. Protein dynamics and allostery: an NMR view. *Curr. Opin. Struct. Biol.* 21:62–67
73. Tzeng SR, Kalodimos CG. 2012. Protein activity regulation by conformational entropy. *Nature* 488:236–40
74. Tzeng SR, Kalodimos CG. 2013. Allosteric inhibition through suppression of transient conformational states. *Nat. Chem. Biol.* 9:462–65
75. Tzeng SR, Pai MT, Kalodimos CG. 2012. NMR studies of large protein systems. *Methods Mol. Biol.* 831:133–40
76. Ullers RS, Ang D, Schwager F, Georgopoulos C, Genevaux P. 2007. Trigger factor can antagonize both SecB and DnaK/DnaJ chaperone functions in *Escherichia coli*. *PNAS* 104:3101–6
77. Ullers RS, Luirink J, Harms N, Schwager F, Georgopoulos C, Genevaux P. 2004. SecB is a bona fide generalized chaperone in *Escherichia coli*. *PNAS* 101:7583–88
78. Verba KA, Wang RY, Arakawa A, Liu Y, Shirouzu M, et al. 2016. Atomic structure of Hsp90–Cdc37–Cdk4 reveals that Hsp90 traps and stabilizes an unfolded kinase. *Science* 352:1542–47
79. Von Eichborn J, Gunther S, Preissner R. 2010. Structural features and evolution of protein–protein interactions. *Genome Inform*. 22:1–10
80. von Heijne G. 1985. Signal sequences: the limits of variation. *J. Mol. Biol.* 184:99–105
81. Whitty A. 2008. Cooperativity and biological complexity. *Nat. Chem. Biol.* 4:435–39
82. Winkler J, Tyedmers J, Bukau B, Mogk A. 2012. Chaperone networks in protein disaggregation and prion propagation. *J. Struct. Biol.* 179:152–60
83. Xu Z, Knafels JD, Yoshino K. 2000. Crystal structure of the bacterial protein export chaperone secB. *Nat. Struct. Biol.* 7:1172–77
84. Zhuravleva A, Clerico EM, Gierasch LM. 2012. An interdomain energetic tug-of-war creates the allosterically active state in Hsp70 molecular chaperones. *Cell* 151:1296–307